JOURNAL OF SOLID STATE CHEMISTRY 135, 282–292 (1998)
ARTICLE NO. SC977638

Synthesis and Crystal Structure Determination of $Tl_8Nb_{27.2}O_{72}$ Using TEM and Single-Crystal X-Ray Diffraction

L. Dupont,*,[1] M. Hervieu,† D. Pelloquin,† G. Nowogrocki,‡ and M. Touboul*

*Laboratoire de Réactivité et de Chimie des Solides, URA CNRS 1211, Université de Picardie Jules Verne, 33 rue Saint-Leu, 80039 Amiens Cedex, France; †Laboratoire CRISMAT, URA CNRS 1318, ISMRA and Université de Caen, 6 Boulevard du Maréchal Juin, 14050 Caen Cedex, France; and ‡Laboratoire de Cristallochimie et Physicochimie du Solide, Université de Lille I, Ecole Nationale Supérieure de Chimie de Lille, B.P. 108, 59652 Villeneuve d'Ascq, France

Received April 17, 1997; in revised form September 18, 1997; accepted September 23, 1997

An investigation of the Nb–Tl–O system has allowed the synthesis of a new phase, $Tl_8Nb_{27.2}O_{72}$. This phase is structurally and chemically close to a Tl–Nb–O phase previously described as a builtup hexagonal bronze with $a \approx 7.4$ Å, $b \approx 13$ Å, $c \approx 7.6$ Å, and an orthorhombic C-type lattice. The electron diffraction study evidences a doubling of the c parameter with regard to the C cell, resulting in an orthorhombic I-type lattice with, in addition, the observation of a second superstructure and twinned microdomains. A structural determination of the mean orthorhombic I-type cell was successfully carried out by combining energy dispersion spectroscopy (EDS) and single-crystal XRD studies and leads to $a = 7.534(7)$ Å, $b = 12.992(12)$ Å, $c = 15.555(12)$ Å, $Z = 8$, space group $Im2m$, $R = 0.097$, and $R_w = 0.099$ from 995 independent reflections. A chemical formula for this thallium niobate, $Tl_8Nb_{27.2}O_{72}$, consistent with EDS results, was deduced by structure refinement. HREM investigations on this phase clearly show irregular occupancy of the supplementary crystallographic positions by niobium atoms together with a monocommensurate modulated structure and twinned microdomains. © 1998 Academic Press

INTRODUCTION

Unlike alkaline niobates, which have been extensively studied, thallium niobates are little known, except for $Tl_2Nb_2O_6$ (1–4). Recently, two papers were published about the simultaneous presence of Tl^I and Tl^{III} (5, 6) in pyrochlore phases such as $Tl_2Nb_2O_{6+x}$. The following monovalent thallium niobates have previously been reported: $Tl_4Nb_6O_{17}$ (4, 7), $Tl_8Nb_{22}O_{59}$ (8), $TlNb_{3+x}O_{9-y}$ (9), $Tl_2Nb_{12}O_{31}$ (4, 10), $TlNb_7O_{18}$ (11), and $Tl_2Nb_{16}O_{41}$ (12). Three of them—$Tl_8Nb_{22}O_{59}$, $TlNb_{3+x}O_{9-y}$, and $TlNb_7O_{18}$—have been the subject of structural study but the results of the structure refinement are not fully satisfactory. For these structures, the chemical formula determined by counting the atoms in the unit cell presents an electroneutrality defect. Several hypotheses have been proposed to explain this charge imbalance: cationic excess, lack of anions, or special arrangements of octahedra. According to Gatehouse (13), this imbalance can also be explained by the presence of fluoride ions coming from appreciable fluorine impurities ($\approx 2\%$) in Nb_2O_5 (14). Gasperin (8, 9, 11) solved the crystal structure of these thallium niobium oxides using the single-crystal X-ray diffraction method. The structures thus deduced from known types presented supplementary thallium and niobium atoms with low occupancies in crystallographic sites never observed before (9, 11). Nevertheless, the charge imbalance always remained and the authors could not reach a conclusion between the different hypotheses.

Thus, it seemed worthwhile to review the study of the Tl–Nb–O system and push as far as possible the structural determination of these compounds. To succeed in our study, we used the complementary techniques of transmission electron microscopy (TEM), energy-dispersion spectroscopy (EDS), and single-crystal X-ray diffraction. The local information obtained with selected-area electron diffraction (SAED) and high-resolution transmission electron microscopy (HREM) complemented and guided the exploitation of statistical results obtained from X-ray diffraction.

The present work deals with the synthesis and structural study of a thallium niobium oxide of $Tl_8Nb_{27.2}O_{72}$ composition. This phase is very close to that described by Gasperin (9) as a thallium niobium oxide of the hexagonal bronze type and with a cation excess ($TlNb_{3+x}O_{9-y}$). Nevertheless, the TEM study reveals the existence of two superstructures that reduce the quality of the X-ray diffracted intensity measurements.

EXPERIMENTAL

Synthesis. The quality of the Nb_2O_5 precursor was checked by microanalysis. No fluorine peak was observed in the EDS diagram.

[1] To whom correspondence should be addressed.

0022-4596/98 $25.00

The $Tl_8Nb_{27.2}O_{72}$ phase was obtained by mixing pure Tl_2CO_3 and Nb_2O_5 with initial ratio 1/2. After manual grinding, the mixture was poured into a platinum crucible and heated under air in a classical furnace. The temperature was first increased (rate 1°C/min) and then stabilized at 300°C during a 12-hr period to allow the thallium carbonate to slowly decompose and to prevent powder puffing during the release of carbon dioxide. The sample was then heated to 1200°C for 6 hr. Finally, the sample was cooled to 100°C at a cooling rate of 2°C/min, resulting in the formation of colorless single crystals. These single crystals did not exhibit a well-defined shape.

Single-crystal measurements. Diffracted intensity measurements were collected with the Philips PW1100 diffractometer of the Centre Commun de Mesure del' Université de Lille I, using Mo$K\alpha$ radiation ($\lambda = 0.7107$ Å) isolated with a graphite monochromator.

The selected crystals were taken out of their mother mixture and mounted at the end of a quartz fiber. A total of 9498 reflections were measured in half the reciprocal space for $2 \leq \theta \leq 30^\circ$ and $-21 \leq h \leq 21$, $-18 \leq k \leq 18, 0 \leq l \leq 10$ in the ω–2θ scan mode.

Electron diffraction and chemical microanalysis study. The electron diffraction (ED) study of the microcrystals was performed with a JEOL 200CX electron microscope fitted with a eucentric goniometer ($\pm 60^\circ$). For all observed microcrystals the Tl/Nb ratio was checked and an electron crystallographic study was carried out.

High-resolution electron microscopy. This study was performed with a TOPCON 002B microscope having a point resolution of 1.8 Å. Image calculations were carried out with the Mac Tempas software. Simulated images were calculated with the positional parameters refined from the XRD pattern for different crystal thicknesses and focus values. Both microscopes are equipped with EDS analyzers (Kevex).

RESULTS AND DISCUSSION

Unit cell parameters and space group determination. The diffracted intensity measurements for the selected crystals led to different results. Although they were deduced from one another, the conditions limiting the reflection and the unit cell parameters were not identical from one crystal to another. The most frequently observed cell parameters are $a = 7.4$ Å, $b = 13$ Å, $c = 7.6$ Å, and $\alpha = \beta = \gamma = 90^\circ$ with the C-type lattice. The other crystals exhibit an I-type lattice and a doubling of the c parameter. To understand the reasons for such differences, we decided to use the ED associated with energy-dispersive X-ray microanalysis to determine the unit cell parameters together with the chemical composition of a crystal.

Electron diffraction and chemical microanalysis study. The EDS analysis performed on numerous crystals did not evidence significant local composition variations. The Tl/Nb ratio is approximately 0.27, and with the hypothesis that all the positive charges are compensated with oxygen, this ratio leads to the chemical formula $TlNb_{3+x}O_{9-y}$. Such a phase was described by Gasperin, and the primary cell parameters obtained by X-ray diffraction fit with the parameters she proposed (9): Orthorhombic system, space group $C222_1$ with $a = 7.551$ Å, $b = 13.005$ Å, $c = 7.734$ Å, $Z = 4$, and $R = 0.0069$ for 535 observed reflections.

The electron diffraction study of the title phase was carried out on numerous crystallites. All of them exhibit a system of intense reflections consistent with the C-type subcell proposed by Gasperin (9) and weaker extra reflections. The reconstruction of the reciprocal space showed that they belong to two different systems:

The first superstructure simply results from the doubling of the c_C axis of the orthorhombic C-type cell. The parameters of the orthorhombic supercell are $a_I = a_C \approx 7.5$ Å, $b_I = b_C \approx 13$ Å, and $c_I = 2c_C \approx 15.2$ Å (a_C, b_C, and c_C being the parameters of the orthorhombic C-type subcell). The conditions limiting the hkl reflections are $h + k + l = 2n$, indicating an I-type lattice. The [001] and [010] ED patterns are given in Figs. la and lb, respectively.

Rotating around the c_C^* axis, a second system of satellites is observed, lying along the $[131]_C^*$ direction. They are clearly observed in the $[\bar{3}10]$ SAED patterns as shown in Fig. 2. The cell parameters of the modulated structure associated with these satellites will be discussed further as well as the relationships with those of the I-type structure.

These observations suggest a high degree of complexity in the atomic arrangement, preventing an accurate structural determination from single-crystal X-ray data for such materials. To alleviate this problem, we worked by coupling HREM and X-ray studies, the latter being carried out in two steps. First, the orthorhombic supercell was taken into consideration, and the structure was investigated from single-crystal X-ray data. Second, the modulated structure was considered.

The Orthorhombic Supercell

Structure refinement. Starting from the approximate subcell parameters, the cell parameters were refined, yielding $a = 7.534(7)$ Å, $b = 12.992(12)$ Å, and $c = 15.555(12)$ Å assuming an I-type lattice. No extra conditions of reflection were observed, leading to $Im2m$, $I222$, and $I2_12_12_1$ as possible space groups.

The choice of the space group was made using the Gasperin structure refinement (9). Indeed, our subcell could be described as two superimposed C-type cells along the c axis. This model (Fig. 3) points out a mirror plane

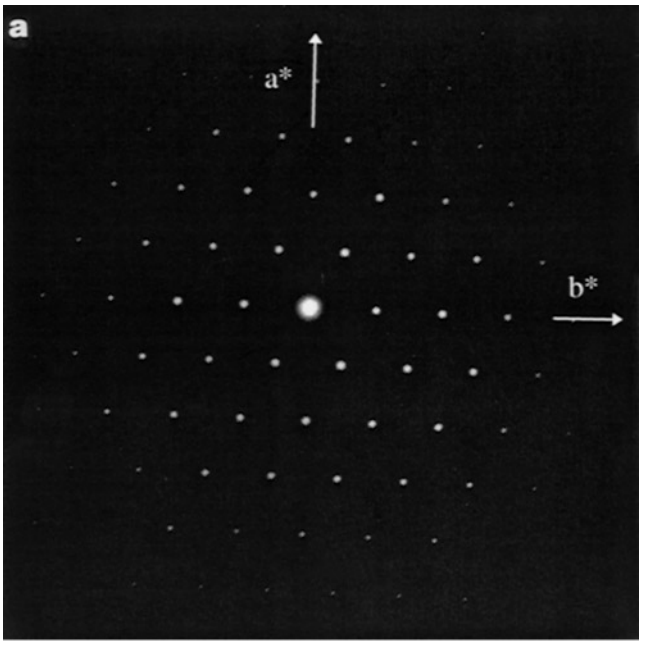

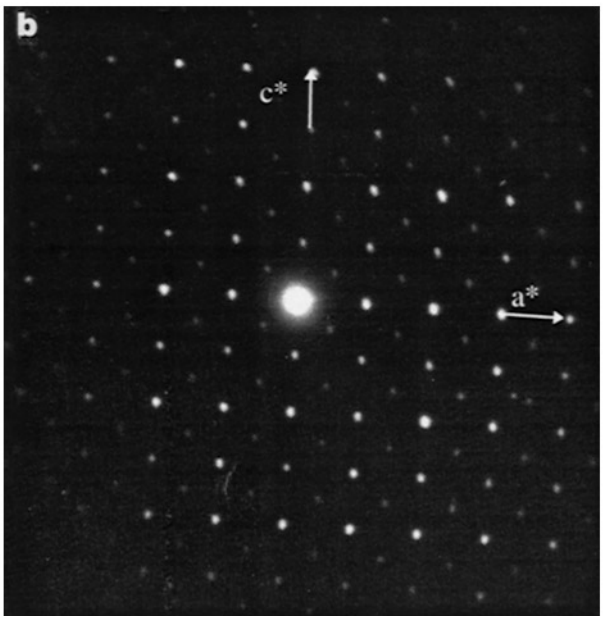

FIG. 1. Electron diffraction patterns of $Tl_8Nb_{27.2}O_{72}$ along the (a) [001] and (b) [010] directions.

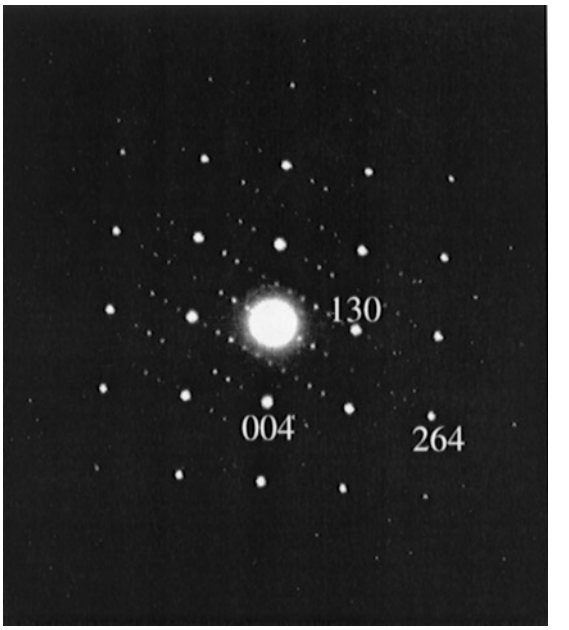

FIG. 2. Electron diffraction pattern of $Tl_8Nb_{27.2}O_{72}$ along the [$\bar{3}$10] direction showing the existence of one set of satellites lying in commensurate positions.

perpendicular to the *c* axis to obtain equivalent atom positions in our cell and in the doubled C cell. The presence of a 2 or 2_1 axis parallel to the *c* axis would imply supplementary atomic positions. Then the space group was assumed to be *Im*2*m* to retain the cell parameters obtained from ED and to have a mirror plane perpendicular to the *c* axis.

Direct methods (15) gave the positions of the heavy atoms, and successive Fourier-difference syntheses provided the positions of the oxygen atoms. The scattering factors used are those of neutral atoms taken from the International Tables for X-ray Crystallography (16). For this refinement, 995 independent reflections were taken, and in spite of the poorly defined shape of the crystal, absorption corrections were applied. Moreover, to relate the difficulty in correctly measuring the diffracted intensities due to the superstructures of microtwinning, two scale factors were determined. The first scale factor was calculated with the even $h + k$, even l reflections corresponding to the C-type lattice (subsubcell); the second was based on odd $h + k$, odd l reflections. The ratio between the two scale factors was refined to 1.588. The final R values are $R = \sum|F_{obs} - F_{calc}|/\sum F_{obs} = 0.097$ and $R_w = (\sum w(F_{obs} - F_{calc})^2/\sum wF_{obs}^2)^{1/2} = 0.099$ and lead to the accurate chemical formula $Tl_8Nb_{27.2}O_{72}$. The positions and thermal motion parameters are reported in Table 1. Significant bond lengths are listed in Table 2.

Description of the structure. As predicted by Gasperin (9), the structure can be directly described as a "hexagonal bronze." The structure skeleton is formed by NbO_6 octahedra sharing their corners. The arrangement of the octahedra creates hexagonal tunnels and triangular prisms parallel to the *c* axis (Fig. 4). The thallium atoms are located in the hexagonal cavities and partially occupy positions shifted from the tunnel center. It is noteworthy that the arrangement of thallium atoms located at $z = \frac{1}{4}$ does not present hexagonal symmetry around the tunnel center (Fig. 5). This fact cannot be explained at the moment but this special arrangement could originate from the structure

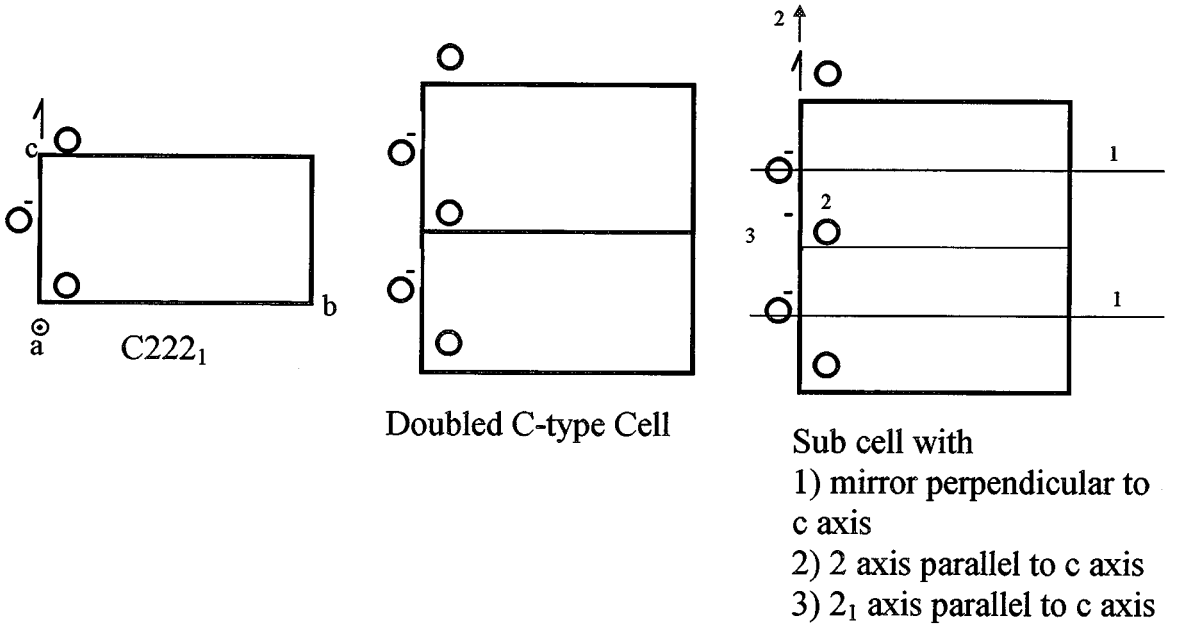

FIG. 3. Model giving an I cell from a doubled C cell.

TABLE 1
Atomic Positions and Thermal Motion Parameters ($\beta_{ij} \times 10^4$)

Atoms	x	y	z	n	B_{eq} or B_{iso}(Å^2)	β_{11}	β_{22}	β_{33}	β_{12}	β_{13}	β_{23}
Nb(1)	0	0.5	0.1221(3)	1	1.22(8)	47(6)	9(2)	20(1)	0	0	7(2)
Nb(2)	0	0.4920(4)	0.3720(4)	1	2.2(1)	48(6)	38(3)	31(2)	0	0	−2(2)
Nb(3)	0.2538(5)	0.2408(4)	0.1288(3)	1	2.02(5)	76(4)	21(1)	30(1)	−4(2)	−25(2)	7(1)
Nb(4)	0.2395(4)	0.7375(4)	0.1219(3)	1	1.77(5)	55(4)	14(1)	32(1)	−13(2)	−10(2)	−10(1)
Nb(5)	0	0.654(1)	0.5	0.475	1.2(2)	57(20)	26(6)	7(3)	0	0	0
Nb(6)	0	0.3285(8)	0	0.625	1.3(2)	16(12)	28(5)	15(3)	0	0	0
Nb(7)	0	0.3254(8)	0.5	0.5	1.2(2)	29(16)	22(5)	14(4)	0	0	0
O(1)	0	0.768(2)	0.104(2)	1	0.6(4)						
O(2)	0	0.448(3)	0.246(1)	1	1.5(5)						
O(3)	0.187(2)	0.596(1)	0.141(1)	1	0.4(2)						
O(4)	0	0.503(3)	0	1	1						
O(5)	0	0.771(2)	0.395(1)	1	0.1(3)						
O(6)	0.5	0.010(3)	0	1	1						
O(7)	0.202(4)	0.205(2)	0	1	1.0(4)						
O(8)	0	0.205(2)	0.148(2)	1	0.7(4)						
O(9)	0	0.204(2)	0.354(2)	1	1.0(4)						
O(10)	0.180(3)	0.381(1)	0.106(1)	1	1.0(3)						
O(11)	0.180(3)	0.381(1)	0.607(1)	1	1.6(4)						
O(12)	0.184(3)	0.595(1)	0.640(1)	1	1.2(3)						
O(13)	0.297(3)	0.705(2)	0	1	0.6(4)						
O(14)	0.215(5)	0.764(2)	0.252(1)	1	3.2(7)						
Tl(1)	0.074(2)	−0.007(2)	0.010(2)	0.06	2.0(4)						
Tl(2)	0.029(2)	−0.040(1)	0.010(1)	0.08	1.6(4)						
Tl(3)	0.028(2)	0.0302(6)	0.009(1)	0.11	1.7(3)						
Tl(4)	0.067(3)	−0.013(2)	0.514(1)	0.06	1.5(4)						
Tl(5)	0.024(2)	−0.0412(6)	0.508(1)	0.14	1.9(2)						
Tl(6)	0.037(3)	0.026(2)	0.515(2)	0.05	2.3(6)						
Tl(7)	0.034(6)	−0.036(3)	0.227(2)	0.05	4.1(9)						
Tl(8)	0.020(9)	−0.018(2)	0.266(2)	0.09	4.8(6)						
Tl(9)	−0.037(1)	0.0110(6)	0.2516(3)	0.36	3.1(1)						

TABLE 2
Interatomic Distances (Å) and Angles (Deg)

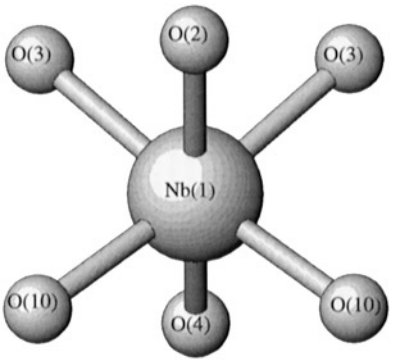

Skeleton niobium and oxygen

Nb(1)	O(10)	O(10)	O(2)	O(3)	O(3)	O(4)
O(10)	2.07(2)					
O(10)	82(2)	2.07(2)				
O(2)	82(2)	82(2)	2.04(2)			
O(3)	91(2)	173(9)	94(2)	1.90(2)		
O(3)	173(9)	91(2)	94(2)	95.6(2)	1.90(2)	
O(4)	84(2)	84(2)	162(5)	98(2)	98(2)	1.90(1)
Nb(2)	O(11)	O(11)	O(6)	O(12)	O(12)	O(2)
O(11)	2.01(2)					
O(11)	85.1(7)	2.01(2)				
O(6)	86(2)	86(2)	2.01(1)			
O(12)	92(2)	175(12)	91(2)	1.94(2)		
O(12)	175(12)	92(2)	91(2)	92(1)	1.94(2)	
O(2)	87(2)	87(2)	170(8)	96(2)	96(2)	2.04(2)
Nb(3)	O(8)	O(5)	O(10)	O(12)	O(7)	O(14)
O(8)	1.99(1)					
O(5)	177(8)	1.93(1)				
O(10)	88(2)	93(2)	1.94(2)			
O(12)	89(2)	89(2)	174(10)	1.96(2)		
O(7)	85(2)	92(2)	89(2)	85(1)	2.09(1)	
O(14)	91(2)	92(2)	94(2)	92(2)	175(10)	1.89(2)
Nb(4)	O(1)	O(9)	O(3)	O(11)	O(13)	O(14)
O(1)	1.87(1)					
O(9)	178(9)	2.05(1)				
O(3)	92(2)	88(1)	1.90(2)			
O(11)	95(2)	86(2)	174(9)	1.97(2)		
O(13)	97(2)	85(2)	89(1)	91(2)	1.99(1)	
O(14)	91(2)	87(2)	89(2)	89(2)	172(8)	2.06(2)

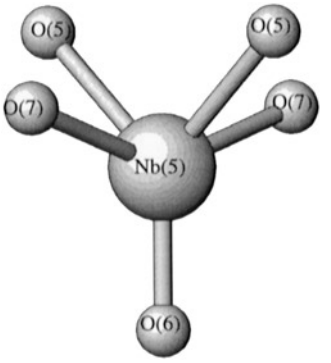

Supplementary Nb(5) in triangular prisms

Nb(5)–O(5)	2.23(3) (×2)
Nb(5)–O(6)	1.87(5)
Nb(5)–O(7)	2.34(3) (×2)

TABLE 2—*Continued*

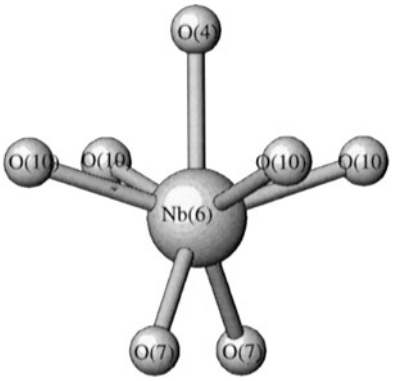

Supplementary Nb(6) in triangular prisms

Nb(6)–O(10)	2.24(2) (×4)
Nb(6)–O(4)	2.27(4)
Nb(6)–O(7)	2.21(3) (×2)

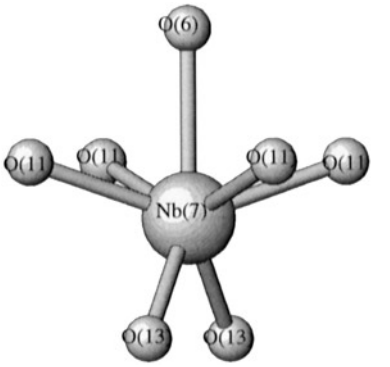

Supplementary Nb(7) in triangular prisms

Nb(7)–O(11)	2.27(2) (×4)
Nb(7)–O(6)	2.40(4)
Nb(7)–O(13)	2.19(2) (×2)

Shortest thallium–oxygen distances

Tl(1)–O(11)	2.80(3)	Tl(2)–O(11)	2.85(3)
Tl(3)–O(7)	2.63(3)	Tl(4)–O(10)	2.75(3)
Tl(5)–O(5)	2.88(3)	Tl(5)–O(10)	2.88(3)
Tl(6)–O(13)	2.65(4)	Tl(7)–O(3)	3.04(6)
Tl(8)–O(14)	2.96(5)	Tl(9)–O(3)	2.89(2)

observed by ED. The supplementary niobium atoms located in the center of the triangular prisms partially occupy this position, and the oxygen neighbors form distorted polyhedra which appear in Fig. 4 as triangular prisms. Moreover, according to Gasperin, due to the observed disorder of the thallium atoms, and in agreement with the ED results, the orthorhombic space group *Im2m* in which this structure has been described must correspond to the lattice of an average cell.

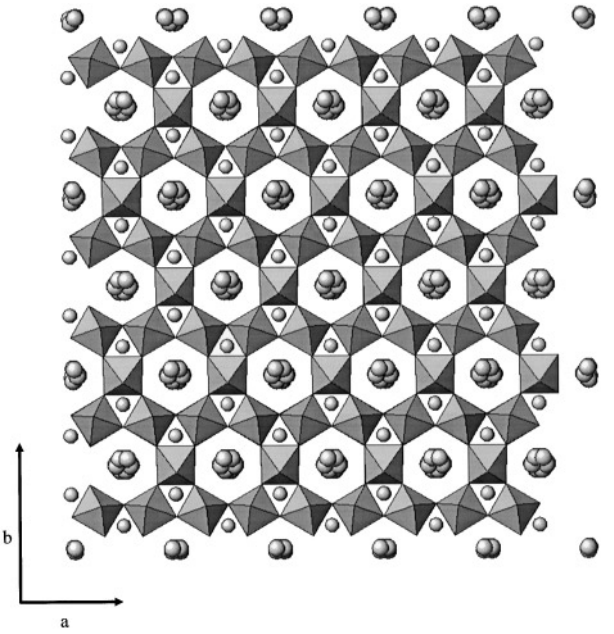

FIG. 4. Structure of $Tl_8Nb_{27.2}O_{72}$ projected along the [001] direction showing skeleton NbO_6 octahedra; thallium atoms and supplementary niobium atoms are shown as spheres.

To understand the origin of the second superstructure, high-resolution electron microscopy was undertaken.

High-resolution electron microscopy along [001]. The interesting point of this structure is indeed the existence of niobium atoms located within the triangular prisms. The best orientation to characterize these additional atoms is [001] since they project over the same point (as well as the thallium atoms located within the hexagonal tunnels).

A [001] enlarged HREM image recorded for a focus value close to the Scherzer value (≈ -250 Å) is given in Fig. 6a; the high electron density zones appear as dark dots. On the crystal edge the contrast consists of a hexagonal array of dark dots. The simulated images calculated for the refined positional parameters (Table 1) and a crystal thickness t close to 15 Å confirm that the dark dots are correlated with the thallium atoms and the niobium atoms located in the octahedral sites. When the crystal thickness increases, the niobium atoms located in the triangular prisms appear as very small dark dots (they are labeled in Fig. 6b and indicated by white arrowheads in Fig. 6a); every type of niobium site is imaged as a dark dot so that the thallium positions appear darker and darker. The contrast at the level of the thallium sites is always highly regular. On the other hand, local variations of contrast are observed at the level of the niobium sites. An example is given in Fig. 7a. In the whole domain, the thallium positions are imaged as very dark dots arranged in a hexagonal array and spaced 7.5 Å, except in the middle of the image (around the arrowhead), where the positions of the niobium atoms in the octahedral sites are almost as dark. Such a feature was

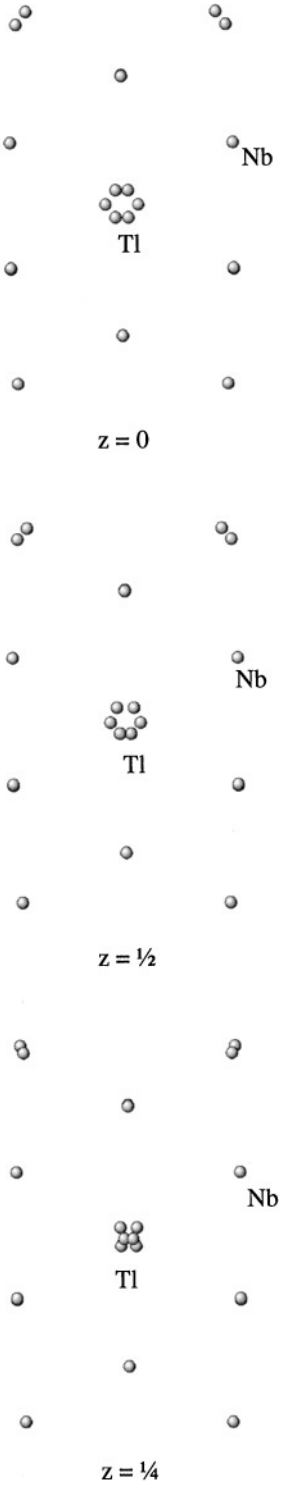

FIG. 5. Arrangement of thallium atoms in the cell at $z = 0$, $z = \frac{1}{2}$, and $z = \frac{1}{4}$.

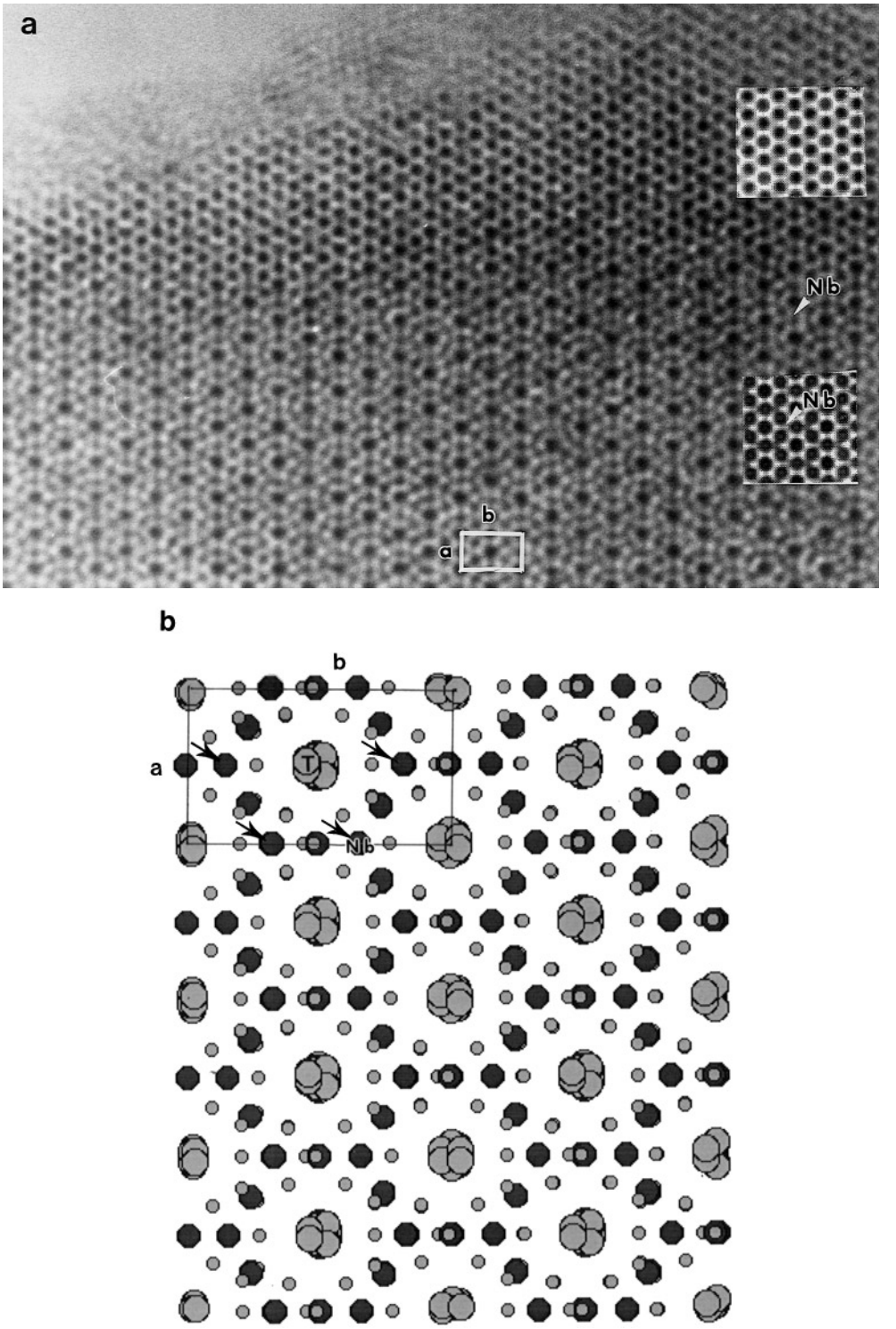

FIG. 6. (a) [001] enlarged HREM image for which the high electron density zones appear as dark dots. The calculated images are superimposed in the right part of the image. (b) Structure of $Tl_8Nb_{27.2}O_{72}$ projected along the [001] direction where the nature of atoms is indicated and where the niobium atoms located in triangular prisms are indicated by arrows.

interpreted by the local absence of niobium atoms in the triangular prism sites; these empty positions appear indeed as bright zones for this focus value (arrowhead). Image calculations confirmed this hypothesis. This contrast variation vs the prismatic site occupation and crystal thickness is illustrated in Figs. 7b and 7c. The theoretical images for

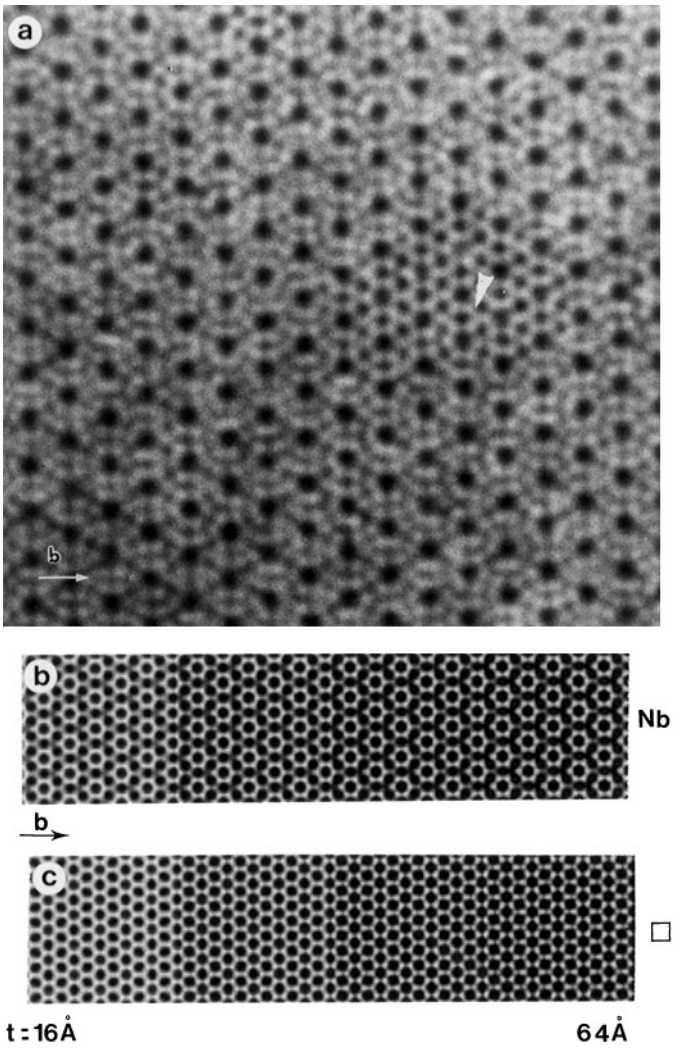

FIG. 7. (a) [001] enlarged HREM image where the niobium atoms located in triangular prisms are indicated by a white arrowhead and the theoretical images calculated for a focus value of -250 Å and a crystal thickness varying from 16 to 64 Å with occupied prisms (b) or empty prisms (c).

a focus value of -250 Å and a crystal thickness varying from 16 to 64 Å are calculated for occupied prisms (Fig. 7b) or empty prisms (Fig. 7c; positional parameters of Gasperin). The variation of contrast is clearly visible with hexagonal dark dots spaced 7.6 Å in the first model and 3.8 Å in the second one.

These observations demonstrate the irregular occupancy of the prisms; however, we are aware of the limits of the models because, as discussed in the next section, the structure is actually modulated. The atomic displacements that could result from such a feature were not taken into account; they are indeed likely to modify the fine contrast but probably not the effect.

The Modulated Structure

As mentioned earlier, the $[\bar{3}10]$ patterns recorded by rotation around c^* (Fig. 2) evidence that a second set of extra spots is systematically present. In this pattern, the satellites lie in commensurate positions along the $[131]^*_C$ direction of the C-type subcell, five satellites being observed along that direction. However, in most of the experimental patterns, additional spots are also observed along the $[\bar{1}31]^*_C$ direction of the C-type subcell (Fig. 8a). In that example, this fact can be interpreted from the existence of two orientational domains, the plane $(1\bar{3}0)_C$ playing the role of a mirror. Taking into account that the C-type structure results from the distortion of a hexagonal ideal cell, the $[131]^*_C$ and $[1\bar{3}1]^*_C$ directions of the C-type orthorhombic cell, as well as $[021]^*_C$, correspond to the equivalent $[11\bar{2}1]^*_H$ directions of the ideal hexagonal cell. As a result, different orientations of the modulation vector are observed since the modulation is established along these equivalent directions. The problem encountered in the reconstruction of the reciprocal space of the modulated structure and the determination of the conditions limiting the reflection arises from the coexistence of these differently oriented domains, probably superimposed with the I-type structure, and that overlap in the course of the crystallite rotation.

It appears that the second system of satellites is therefore generated by a modulated phase that is commensurate. Considering the appearance of the satellites in the monodomains and the fact that the direction of the modulation vector is not parallel to the crystallographic axes, the modulated character of the superstructure must be expressed in a first analysis of a simple monoclinic cell. Taking into account that the different directions of modulation result from pseudosymmetry effects with regard to the hexagonal (and orthorhombic) subcell, the a^*_m, b^*_m, and c^*_m vectors of the reciprocal monoclinic cell correspond to the $[100]^*_H$ (i.e., a^*_C or $[130]^*_C$), $[1\bar{2}10]^*_H$ (i.e., b^*_C or $[1\bar{1}0]^*_C$), and $[001]^*_H$ (i.e., $[001]^*_C$) axes, respectively. This is summarized in Table 3. The parameters of the monoclinic cell are

$$a_m \approx 7.5 \text{ Å} \approx a_C \approx 2d_{130}, \quad b_m \approx 13 \text{ Å} \approx b_C \approx 2d_{1\bar{1}0},$$

$$c_m \approx 2c_C, \alpha = \beta = 90^\circ, \quad \gamma \approx 90^\circ,$$

where the subscript m refers to the modulated monoclinic cell. All order satellites can therefore be indexed by a modulation vector with $q = \frac{1}{3}a^*_m + \frac{1}{3}c^*_m$.

To describe the HREM results, the indexation mode of the orthorhombic cell is retained. A $[\bar{3}10]$ HREM image recorded for a focus value close to -250 Å, where low electron density zones are imaged as bright spots, is given in Fig. 8b. In the thin part of the crystal edge, the contrast consists of an almost square array of bright dots, aligned along [130] and [001] and spaced ≈ 3.85 Å. This contrast

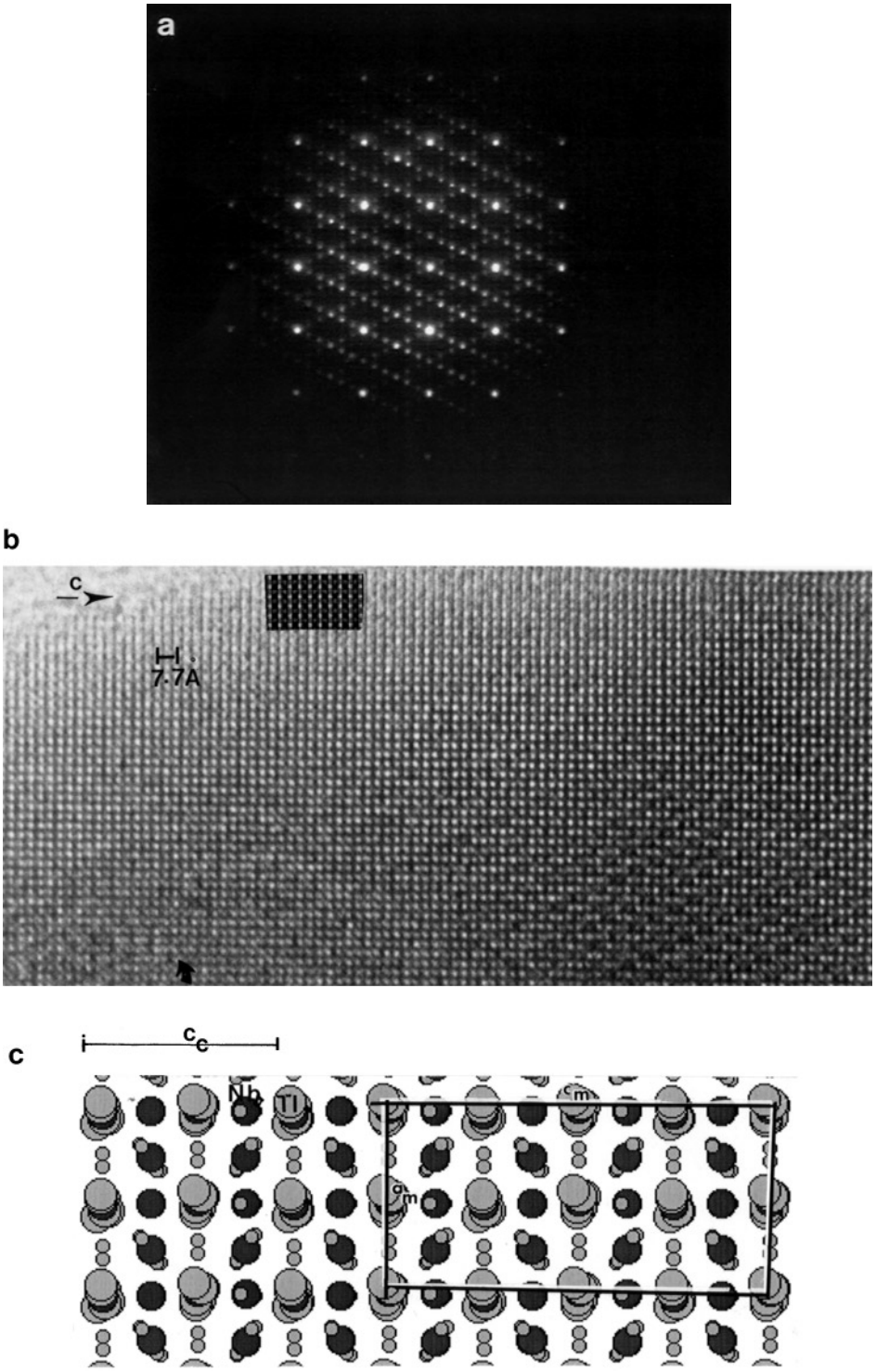

FIG. 8. (a) Electron diffraction pattern showing additional spots along $[\overline{1}31]^*_C$. (b) $[\bar{3}10]$ HREM image where low electron density zones are imaged as bright spots. The calculated image is superimposed at the bottom left of the image. (c) Corresponding projected structure where the nature of atoms is indicated and the projected monoclinic cell is superimposed.

fits with that of the orthorhombic C-type structure, the dark spots corresponding to the projected positions of thallium and niobium atoms; the simulated image, calculated using the positional parameters of the C-type structure and a crystal thickness of 26 Å, is inserted at the top of the micrograph, and the atom projections are given in Fig. 8c. As the crystal

TABLE 3
The Equivalent Directions of the Different Lattices

Hexagonal	Orthorhombic C	Orthorhombic I	Monoclinic
$[100]^*_H$	$[100]^*_C$ and $[130]^*_C$	$[100]^*_I$ and $[130]^*_I$	a^*_m
$[1\bar{2}10]^*_H$	$[010]^*_C$ and $[1\bar{1}0]^*_C$	$[010]^*_I$ and $[1\bar{1}0]^*_I$	b^*_m
$[001]^*_H$	$[001]^*_C$	$[001]^*_I$	c^*_m

thickness increases, variations in the contrast are observed. In the right side of the image, contrast modulations are clearly visible. Viewing the image at grazing incidence clearly shows that these variations are associated with variations of both brightness and positions of the white and dark dots; the periodicity along [001] is six times the c_C parameter (i.e., three times the c_m parameter of the modulated structure), and that along [130] is six times the d_{130} parameter (i.e., three times the a_m parameter). Note that on the bottom left of Fig. 8b variations of contrast are also locally observed (curved arrow), which are associated with variations of the interdot distances along [001] but they do not occur in a periodic way.

Figure 9 is an overall image where four oriented domains are observed, which are numbered from 1 to 4. In domains 2 and 4, the modulation directions are parallel whereas the orientation of the wave vector changes and domain 3 is a twinning modulated domain. Note that the domain boundaries are not planar. Viewed along that direction, no modulation is visible in area 1; this contrast may be due either to another (and equivalent) orientation of the modulation or to the disappearance of this modulation. It is

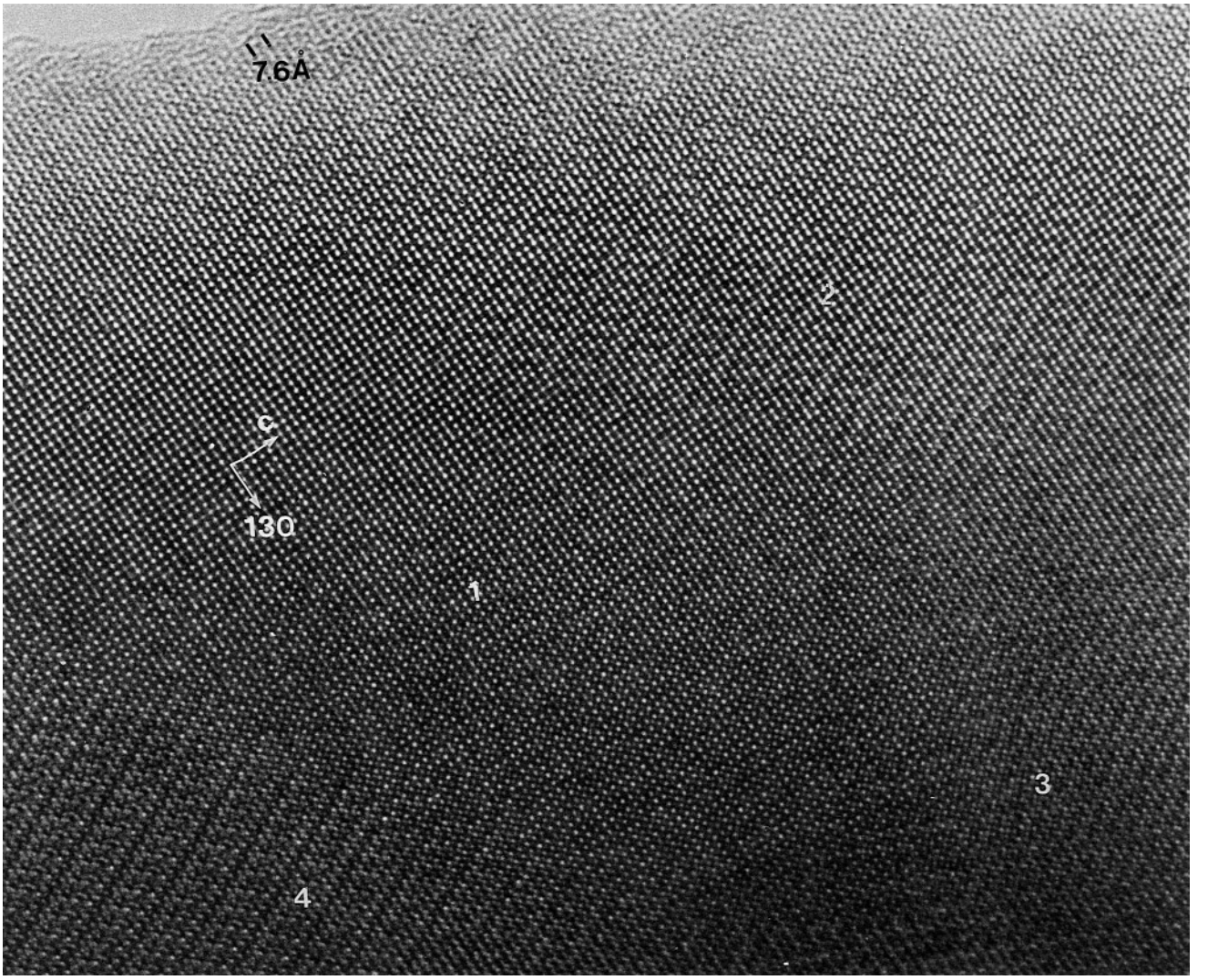

FIG. 9. $[\bar{3}10]$ overall HREM image where four oriented domains numbered from 1 to 4 are observed.

important to note that the crystallites are made of small twin domains and that the periodicity of the modulation always corresponds to the expected one. This is in agreement with the sharpness of the satellites in the electron diffraction pattern. In a general way, the twinning domains (a few tens or a hundred nanometers wide) are too small to be observed with a light microscope with polarized light.

ED and HREM studies of $Tl_8Nb_{27.2}O_{72}$ allowed observation of a monocommensurate modulated structure. Due to the complexity of the projected structure along the $[\bar{3}10]$ direction, it is indeed impossible to propose a model for the modulated structure but the images suggest an occupancy and displacive modulation. However, the high regularity of the periodicity should allow refinement of the modulated structure from single-crystal X-ray data; this study is in progress.

CONCLUDING REMARKS

This study has shown the high degree of complexity in the position of the atoms within the thallium–niobium oxide structure, explaining the difficulties encountered in accurately solving the structure of such phases from single-crystal X-ray data. The complexity was further confirmed by a TEM study. Nevertheless, this study provided clear evidence of the existence of superstructures and twinned domains as well as insights into their origin. Due to the existence of two different superstructures, the $Tl_8Nb_{27.2}O_{72}$ cell originally described with the orthorhombic C-type lattice was shown to be better described with a monoclinic lattice. Following these observations, the structure was first investigated from single-crystal X-ray data with the orthorhombic I-type supercell with a monocommensurate modulated structure as evidenced by ED and HREM investigations. This modulated structure seems to be due to an occupancy and displacive modulation. A structure refinement from single-crystal X-ray data currently in progress should confirm this hypothesis. On the basis of these findings that Tl–Nb–O compounds are prone to favor structure modulations, other phases within the ternary phase diagram are being investigated.

REFERENCES

1. J. L. Fourquet, G. Ory, G. Gauthier, and R. Pape, *C. R. Acad. Sci. Paris* **271**, 773 (1970).
2. J. L. Fourquet and R. Pape, *Mater. Res. Bull.* **8**, 393 (1973).
3. N. Ramadass, T. Palanisamy, J. Gopalakrishnan, G. Aravamudan, and M. V. C. Sastri, *Solid State Commun.* **17**, 545 (1975).
4. I. N. Belyaev, T. G. Lupeiko, V. B. Nalbandyan, and E. V. Abania, *Russ. J. Inorg. Chem.* **22**, 1702 (1977).
5. J. L. Fourquet, H. Duroy, and Ph. Lacorre, *J. Solid State Chem.* **114**, 575 (1995).
6. H. Mizogushi, H. Kawazoe, T. Ueda, S. Hayashi, H. Hosono, and N. Ueda, *Bull. Chem. Soc. Jpn.* **69**, 111 (1996).
7. I. N. Belyaev, V. B. Nalbandyan, I. L. Trubnikov, and B. S. Medvedev, *Russ. J. Inorg. Chem.* **29**, 144 (1984).
8. M. Gasperin, *Acta Crystallogr., Sect. B: Struct. Crystallogr. Cryst. Chem.* **33,** 398 (1977).
9. M. Gasperin, *Acta Crystallogr., Sect. B: Struct. Crystallogr. Cryst. Chem.* **33,** 2306 (1977).
10. I. N. Belyaev and V. B. Nalbandyan, *Zh. Neorg. Khim.* **28,** 2154 (1983).
11. V. Bhide and M. Gasperin, *Acta Crystallogr., Sect. B: Struct. Crystallogr. Cryst. Chem.* **35,** 1318 (1979).
12. C. D. Whiston and A. J. Smith, *Acta Crystallogr., Sect. B: Struct. Crystallogr. Cryst. Chem.* **34,** 1454 (1978).
13. B. M. Gatehouse, D. J. Lloyd, and B. K. Miskin, in "Proceedings of the 5th Materials Research Symposium," vol. 364, p. 15. 1972.
14. S. Andersson and A. Aström, *Acta Chem. Scand.* **18,** 2233 (1964).
15. G. M. Sheldrix, "SHELX-76: A Program for Crystal Structure Determination." Univ. of Cambridge, 1976.
16. "International Tables for X-ray Crystallography," Vol. IV. Kynoch Press, Birmingham, 1974. [Present distributor: Kluwer Academic, Dordrecht]